

# OPERATIONAL LIMITS OF HIGH DENSITY H-MODES IN ASDEX Upgrade

V. Mertens, K. Borrass, M. Kaufmann, P.T. Lang, R. Lang, H.W. Müller, J. Neuhauser, R. Schneider, J. Schweinzer, W. Suttrop, ASDEX Upgrade Team

Max-Planck-Institut für Plasmaphysik, EURATOM-IPP Association,  
Garching und Berlin, Germany

## Abstract

Systematic investigations of H-mode density limit (H→L-mode back transition) plasmas with gas fuelling and alternatively with additional pellet injection from the magnetic high-field-side HFS are being performed in the new closed divertor configuration DV-II. The resulting database covering a wide range of the externally controllable plasma parameters  $I_p$ ,  $B_t$  and  $P_{heat}$  confirms that the H-mode threshold power exceeds the generally accepted prediction  $P_{heat}^{L→H} \propto \bar{n}_e B_t$  dramatically when one approaches Greenwald densities. Additionally, in contrast to the Greenwald scaling a moderate  $B_t$ -dependence of the H-mode density limit is found. The limit is observed to coincide with divertor detachment and a strong increase of the edge thermal transport, which has, however, no detrimental effect on global  $\tau_E$ .

The pellet injection scheme from the magnetic high-field-side HFS, developed recently on ASDEX Upgrade, leads to fast particle drifts which are, contrary to the standard injection from the low-field-side, directed into the plasma core. This improves markedly the pellet particle fuelling efficiency. The responsible physical mechanism, the diamagnetic particle drift of the pellet ablatant was successfully verified recently. Other increased particle losses on respectively different time scales after the ablation process, however, still persist. Generally, a clear gain in achievable density and plasma stored energy is achieved with stationary HFS pellet injection compared to gas-puffing.

## 1. Introduction

In order to achieve thermonuclear burn, future fusion experiments must safely operate at rather high density, while retaining sufficiently high energy confinement. Since present reactor concepts base on H-mode confinement, the accessibility of the H-mode at the desired high densities has to be demonstrated. Present experiments, however, show that the useful tokamak operation space is limited towards high density by various processes, such as excessive edge radiation cooling, the onset of MHD instabilities (e.g. ballooning limit), detachment or simply by intolerable energy confinement degradation (e.g. loss of H-mode, called here 'H-mode density limit'). The empirically gained heating power independent Greenwald density limit scaling,  $\bar{n}_e^{GW} \propto I_p / a^2 \propto B_t / (q_\psi R)$  [1], which primarily has been developed for OH and L-mode discharges, was found to be quite successful in describing experimental data.

As often demonstrated injection of cryogenic pellets is a successful tool to surpass the Greenwald limit. However, past experiments have revealed that in the ELMy H-mode the pellet particle fuelling efficiency degrades strongly with increasing heating power. This holds for the standard injection scheme from the magnetic low field side (LFS).

During the short process of pellet ablation these particles build a short living high pressure plasmoid which is subject to a diamagnetic force. This force points radially outwards. Therefore we altered our system to inject pellets from the inner side of the torus, i.e. from the magnetic high field side (HFS) [2]. This new injection scheme leads to significantly improved instantaneous particle fuelling efficiency while the density build-up in the plasma may be still governed by transport degradation phenomena thereafter.

In the first part the paper presents parameter dependencies of the H-mode density limit with large variation of the externally controllable parameters plasma current, toroidal magnetic field and heating power. In the second part, the advantages of the novel HFS pellet injection scheme on plasma performance is discussed.

## 2. Discharge Parameters

Our investigations concentrated on lower single null discharges ( $R = 1.65$  m,  $a = 0.5$  m,  $\kappa \sim 1.6$ ,  $\delta \leq 0.2$ ) in deuterium with plasma currents  $I_p$  of 0.4-1.2 MA and toroidal magnetic fields  $B_t$  of 1.3-3 T, corresponding to edge safety factors  $q_{95}$  between 3 and 11. NBI heating powers up to 15 MW have been applied.  $\bar{n}_e$  ranged from  $0.5 \cdot 10^{20} m^{-3}$  to  $1.7 \cdot 10^{20} m^{-3}$ .

The pellet experiments were performed at one particular plasma current of 0.8 MA. The deuterium pellets were injected from the upper HFS with an inclination angle of  $\approx 44^\circ$  with respect to the midplane directed towards the plasma centre [3]. Current technical configurations of the centrifuge temporarily limited the achievable pellet velocity and repetition rate to 240 m/s and 60 Hz, respectively. The related particle flux of  $\Phi \approx 10^{22} D/s$  corresponds to a strong gas-puff by means of external valves. In density feed-back mode the 'dead time' connected with the centrifuge rotation frequency of about 80 ms results in noticeable density oscillations. The ongoing increase in pellet velocity will molder this disadvantage.

## 3. High Density Operation with Pure Gas-puffing

### 3.1. Experimental Phenomenology of High Density H-modes

The H-mode is generally accessible when the input heating power  $P_{heat}$  exceeds a certain limit depending on density and magnetic field  $P_{heat}^{L \rightarrow H} = c \cdot \bar{n}_e B_t$  where the constant  $c$  depends primarily on ion species and ion  $\nabla B$  drift direction. The back-transition H  $\rightarrow$  L-mode shows the same parameter dependencies but occurs at about half the threshold power  $P_{heat}^{L \rightarrow H}$  [4]. Closely above the H-mode is characterized by high frequency type-III ELM's ( $\partial \nu_{ELM} / \partial P_{heat} < 0$ ), but well above the threshold the ELM activity changes to lower frequency type-I ELMs ( $\partial \nu_{ELM} / \partial P_{heat} > 0$ ) [5].

During density build-up of H-mode plasmas up to the non disruptive H-mode density limit the discharges normally pass the following phases : the ELM frequency rises and at high density the ELM's revert from type-I back to type-III. The density at the separatrix  $n_e^{sep}$  increases monotonically with  $\bar{n}_e$  but tends to saturate in the high density type-III ELM phase despite an increasing neutral particle flux. Divertor detachment sets in firstly at the separatrix between type-I ELM's at high densities and develops clearly further during the type-III ELM phase. In parallel, the H-mode pedestal edge pressure gradient which approaches the ideal ballooning limit in the type-I ELM phases decreases slightly with the appearance of type-III ELM's. Taking the practically constant edge density and neglecting the small variation of the power across the separatrix  $P_{sep} = P_{heat} - P_{rad}^{bulk}$ , the measured drop in  $\nabla T_e$  can be interpreted as an enhancement of the edge transport, i.e. a significant rise of the effective perpendicular electron transport coefficient  $\chi_{e,\perp}^* \propto P_{sep} / (n_e \nabla T_e)$  [7]. It is important to note that although  $\chi_{e,\perp}^*$  increases strongly at the plasma edge, this has no immediate deleterious effect on the global  $\tau_E$  [6-9]. The confinement degrades smoothly during the entire density rise to L-mode levels. In parallel, the electron temperature closely inside the separatrix at the H-mode transport barrier approaches  $\approx 150$  eV at the density limit, indicating that the loss of H-mode is a lower edge temperature limit [20]. If  $\bar{n}_e$  is increased further after the H  $\rightarrow$  L-mode transition the separatrix temperature drops further, a Marfe forms close to the X-point and the discharge disrupts.

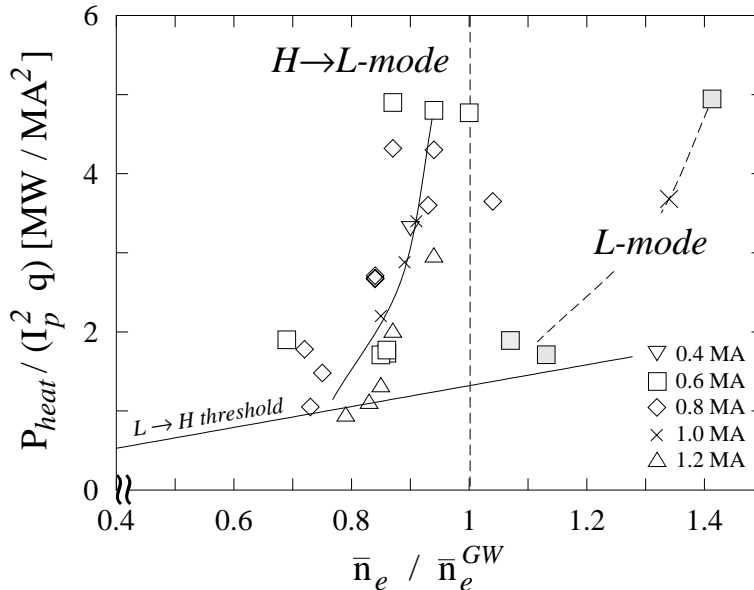


Figure 1: The operation diagram shows the strong deviation of the power needed to achieve H-mode close below  $\bar{n}_e^{GW}$  from the usual  $P_{heat} \propto \bar{n}_e B_t$  scaling.

### 3.2. H-mode Limit Parameter Dependencies

#### 3.2.1. Global Parameters

Approaching the Greenwald limit the L $\leftrightarrow$ H-mode threshold power is found to deviate from the above scaling and rises dramatically, see Figure 1. This means that the H-mode density limit becomes nearly independent of  $P_{heat}$ . Additionally, the L $\leftrightarrow$ H-mode hysteresis is vanished. Earlier experiments on ASDEX Upgrade have shown this detrimental effect at one particular plasma current of  $I_p = 0.8$  MA [13].

To get more confidence into the validity of the deviation, further parameter scans have been performed, especially in  $I_p$ ,  $B_t$  and  $P_{heat}$ . Figure 1 gives an overview over these experiments. To combine the data of different  $I_p$  in one picture with the common H-mode threshold scaling we introduce a first approximation and replace  $\bar{n}_e$  by normalized densities  $\bar{n}_e / \bar{n}_e^{GW}$  in the  $P_{heat} \propto \bar{n}_e B_t$  expression. This leads to  $P_{heat} / (I_p^2 q_{95}) \propto \bar{n}_e / \bar{n}_e^{GW}$ . Figure 1 demonstrates clearly that the earlier findings [13] hold also for the significantly enlarged parameter space. It is interesting to note that the increase of  $I_p$  by a factor of 3 yields roughly the same normalized densities  $\bar{n}_e / \bar{n}_e^{GW}$ , i.e. at 1.2 MA three times the line averaged density than at 0.4 MA. This is noticeable since the large density variation implies, in parallel, a strong modification of the particle fuelling profiles for both, recycling and NBI heating sources. One can suspect that the particle fuelling profile shape has no strong effect on the loss of the H-mode. Normally, with gas-puffing alone the Greenwald limit is not exceeded. In the L-mode, however, it can clearly be surpassed; see Fig. 1.

To get deeper insight into the H-mode limit physics we performed a detailed fit to the database. The wide parameter variation might also allow for the discrimination between different density limit models. The experiments are well described by the empirical regression fit :

$$\bar{n}_e^{exp} = 5.0 \frac{q_{\perp}^{0.15} B_t^{0.61}}{(q_{\psi} R)^{0.95}}$$

[ $10^{20} \text{m}^{-3}$ ,  $\text{MWm}^{-2}$ , T], where  $q_{\perp} = P_{sep}/S$  and  $S$  is the plasma surface. It is remarkably close to the scaling following scaling proposed in [14]

$$\bar{n}_e^{BLS} = 4.14 \frac{q_{\perp}^{0.09} B_t^{0.53}}{(q_{\psi} R)^{0.88}}$$

which relates the H-mode density limit to divertor detachment. We also compared our findings with the Greenwald scaling

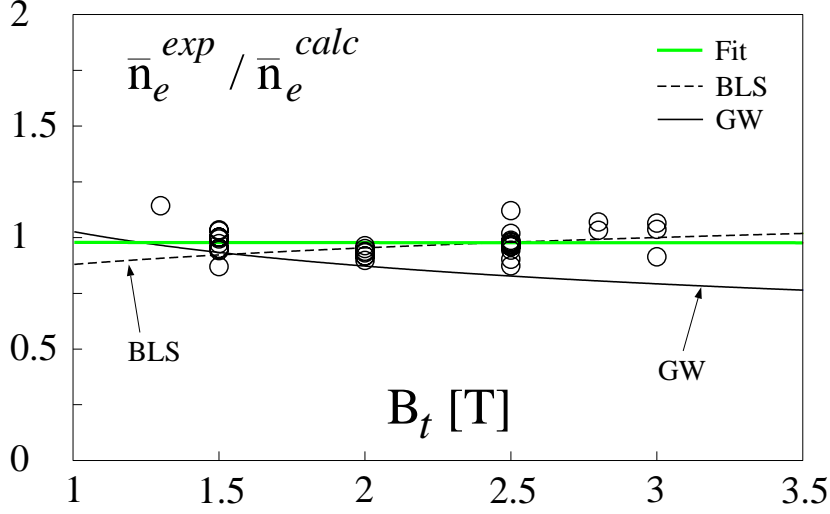


Figure 2:  $\bar{n}_e^{exp} / \bar{n}_e^{calc}$  versus  $B_t$  for ASDEX Upgrade data (circles). The experimental data are normalized by the three different scalings and the fit through each data set is plotted. The parameter dependencies are described in the text. A clear difference is seen between the empirical fit  $\bar{n}_e \propto B_t^{0.6}$  and the Greenwald scaling  $\bar{n}_e \propto B_t$ .

$$\bar{n}_e^{GW} = \frac{I_p}{\pi a^2} \equiv 1.59 \frac{B_t}{q_\psi R} g$$

[ $10^{20} \text{m}^{-3}, \text{MA}, \text{m}, \text{T}$ ] where  $g$  is determined by the plasma shape and held constant in our experiments.

While the first two scalings virtually coincide on the existing database, the deviations from the Greenwald scaling can be reliably assessed. This is particularly true of the  $B_t$  dependence which is clearly weaker than in the Greenwald scaling, as illustrated in Fig. 2.

In edge based models the  $B_t$  dependence is directly related to the  $B_t$ -dependence of the underlying transverse scrape-off layer transport (BLS scaling). The wide  $B_t$  variation in the present database offers for the first time the possibility to discriminate between various alternative transport models.

### 3.2.2. Local Edge Parameters

The density profiles are very flat in the bulk and steep in the edge region, as shown in Fig. 3 b). During the  $\bar{n}_e$  rise the ratio  $n_e^{sep} / \bar{n}_e$  increases but in the at least partly detached type-III

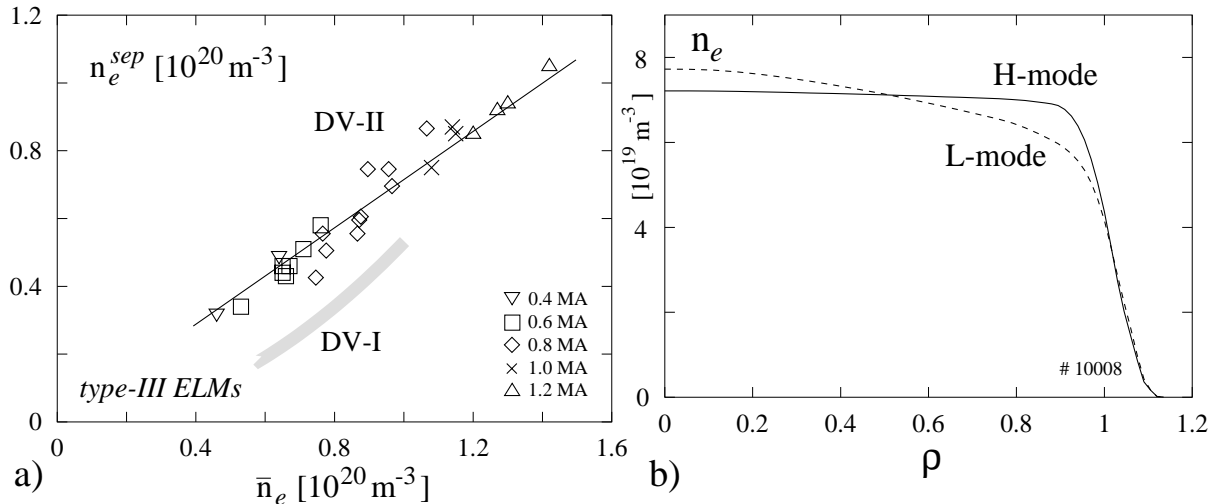


Figure 3: The Figure demonstrates a strong density profile similarity at the H-mode density limit. The corresponding density profiles in DV-I are analyzed only at  $I_p = 0.8 \text{ MA}$ . The L-mode profile is drawn for comparison.

ELM phase close to the density limit the ratio reaches a constant value independently of the absolute  $\bar{n}_e$ , i.e. the profiles there are strongly self-similar over a wide density range as seen in Fig. 3 a). This is different to findings in the open divertor DV-I, where  $n_e^{sep}$  increased roughly quadratically with  $\bar{n}_e$ . Also the edge densities at a given  $\bar{n}_e$  were clearly lower [13,17]. The latter holds not only for the high density H-mode but also for practically all other plasma modes in DV-II [17]. The weak power dependence of the separatrix density  $n_{sep}/I_p \propto P_{sep}^{0.2}$  found in DV-I [13] is preserved in DV-II.

### 3.3. High Density Operation with HFS Pellet Injection

Particle deposition deep inside the separatrix, in H-mode plasmas inside the transport barrier, qualitatively differs from gas-puffing acting primarily at the edge. But strong pellet particle fluxes applied to achieve high plasma densities are always accompanied by strong parasitic gas-puffs originating from the outflowing pellet particles, especially for LFS injection. Since high recycling leads to energy confinement degradation, the physics of the pellet particle losses is investigated with the aim to avoid them.

First, short time phenomena affecting the particle fuelling profile during the pellet ablation are discussed. Thereafter, long term aspects during high density steady state pellet fuelling are presented.

#### 3.3.1. Fast Particle Drifts During Pellet Ablation

Pellets injected into a hot plasma sublimate and a neutral gas cloud is forming around the pellet [18]. Due to the incoming electron heat flux the gas is ionized and the plasmoid of cold, dense plasma expands along the magnetic field lines in  $\mu\text{s}$  time scale [11]. Due to shielding effects the ablation is strongly modulated [16]. Measurements showed a mean plasmoid density of  $3 \cdot 10^{23} \text{m}^{-3}$  and temperature of 2 eV in an ohmic discharge being in good agreement with measurements in other tokamaks [10]. Since the heating electrons are much faster than the expanding plasmoid ions the plasmoid acts as an energy sponge and its normalized pressure  $\beta \propto n T/B^2$  rises quickly despite energy losses due to ablation, ionization, and radiation. This localized high- $\beta$  plasmoid is diamagnetic with respect to the surrounding plasma. The related acceleration  $a_D$  in an inhomogenous field to the LFS of  $a_D \propto T / (mR) \sim 10^9 \text{ms}^{-2}$  [12] drives velocities up to  $10^3 \dots 10^4 \text{m/s}$ .

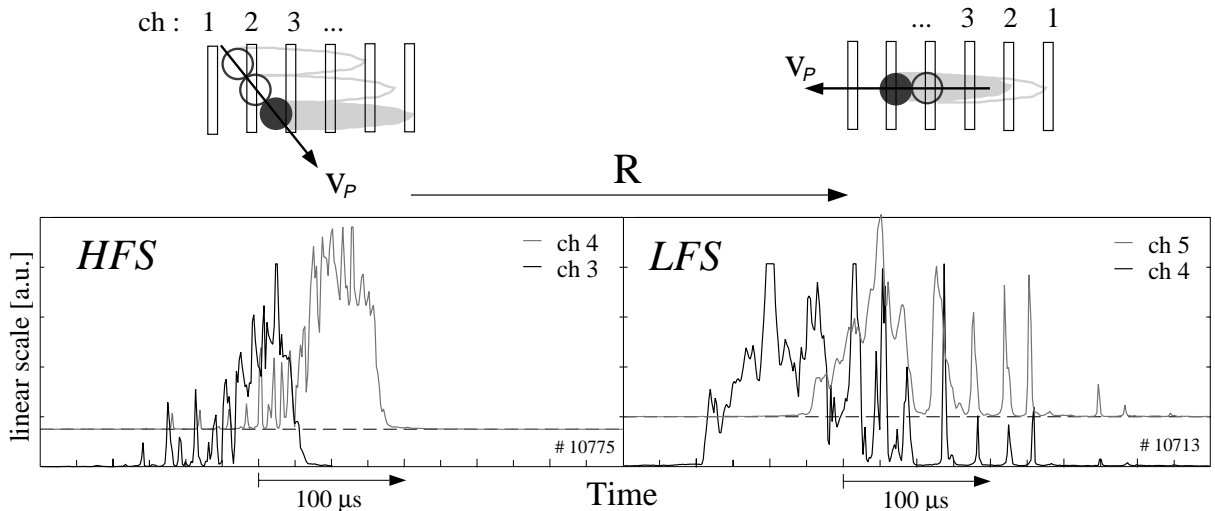


Figure 4: Comparison of the ablation and drift behaviour of HFS and LFS injected pellets in bremsstrahlung emissivity. The pronounced spikes correspond to the fast drifting plasmoids and the broad peaks to the pellet ablation itself. The geometry of the observation channels is sketched in the top.

In recent experiments this high- $\beta$ -drift was measured for the first time highly resolved in radius and time. Both ablation paths (HFS and LFS) are observed by 10 radially separated

channels, as shown in Figure 4. This Figure gives an example of the bremsstrahlung emissivities (538 nm) of one HFS and one LFS pellet, respectively. In the case of LFS injection the signals start with a broad peak followed by pronounced spikes. This behaviour is different with HFS injection. Here the detected radiation starts with several increasing spikes and ends in a broad peak. This is, in fact, what one expects in case of ablation plasmoids accelerated in major radius direction: In LFS injection first the pellet pass one line of sight. Therefore the main peak is associated with the radiation which originates directly from the ablation cloud surrounding the pellet which slowly passes the line of sight. The spikes afterwards correspond to fastly backwards drifting plasmoids. The separation of the spikes is thought to be caused by the well known fluctuation in the ablation rate [10]. In the case of pellet injection from the HFS drifting plasmoids moving ahead the pellet cross the viewing channel before the broad ablation peak follows. The plasmoid velocities and direction deduced from the spikes agree well with theoretical estimates. The particles quickly lost from the plasma during LFS injection are favourably pushed towards the plasma core during HFS injection. Principally, additional particle loss is caused a few ms after injection by pellet induced ELM's [15].

### 3.3.2. Steady State HFS Pellet Fuelling

The main aim of our experiments was demonstration of density feed-back steady state operation close to or even beyond  $\bar{n}_e^{GW}$  with clear H-mode characteristics. The target plasma conditions were varied mainly by changing the external gas-puff rate, pumping speed (e.g. by cryopumping) and the preprogrammed density  $\bar{n}_e^{set}$ . In the course of the experiments it was found that the global confinement characteristics of purely gas refuelled discharges were preserved during the pellet fuelling phase. The actual peak density  $\bar{n}_e$ , e.g., decayed after each pellet towards the equilibrium value  $\bar{n}_e^{equ}$  found in equivalent discharges without pellet injection. The density evolution after the injection of a pellet can be described by the expression:

$$\bar{n}_e(t) = \bar{n}_e^{equ}(t_0) + Ae^{-(t-t_0)/10ms} + (\Delta - A)e^{-(t-t_0)/120ms}.$$

The fastly decaying component of 10 ms specifies the loss of approximately half of the pellet mass ( $A \approx 1 \cdot 10^{19}m^{-3}$ ).  $\Delta$  is the required density enhancement  $\bar{n}_e^{set} - \bar{n}_e^{equ}$  and  $t_0$  is the injection time. This suggests that the pellet induces a short lasting ( $\approx 10$  ms) increase of particle transport, probably by enhanced turbulence. The slow component of 120 ms corresponds to the usual bulk particle confinement.

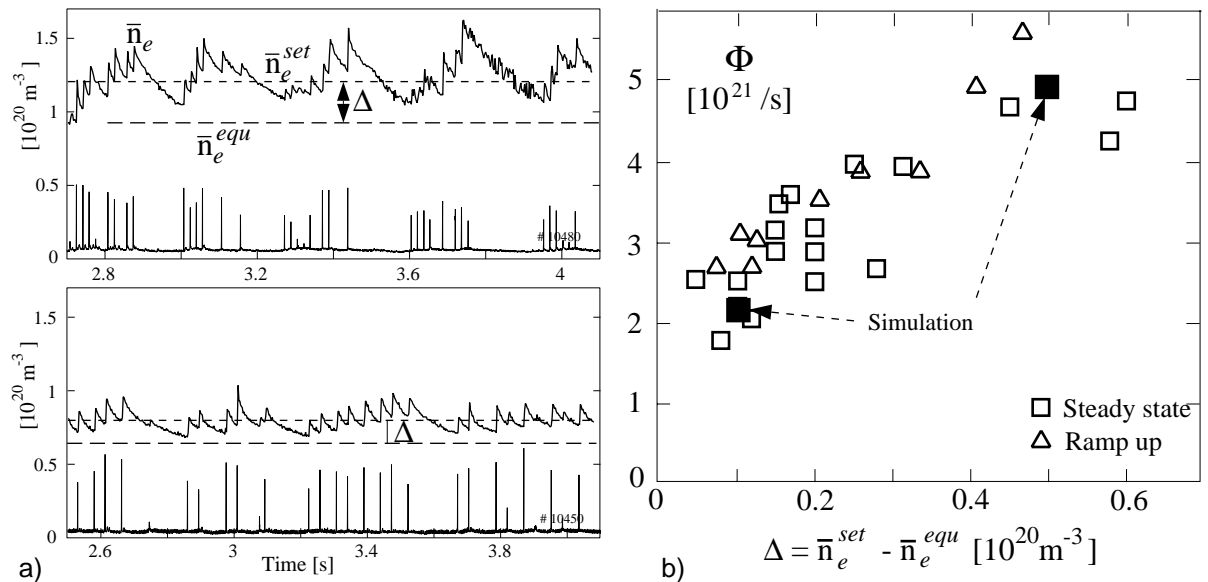


Figure 5: Two examples of steady state HFS pellet fuelled discharges. The needed pellet flux  $\Phi$  depends on the requested density excess  $\Delta$ , independently of its distance to  $\bar{n}_e^{GW}$ .  $\bar{n}_e^{GW}$  is here  $1 \cdot 10^{20}m^{-3}$ .

Injection at a sufficiently high pellet frequency can raise the density to the requested level

$\bar{n}_e^{set}$ . The density enhancement  $\Delta$ , however, determines the required pellet particle flux, irrespectively of the initial plasma conditions. This behaviour is shown in Figure 5 a), where  $\bar{n}_e$  time traces are shown for discharges with different initial conditions and different  $\bar{n}_e^{set}$ . In Figure 5 b) the required pellet particle flux is plotted versus  $\Delta$  for the whole database. The approximately linear increase of the required pellet particle flux  $\Phi$  with density increment  $\Delta$  indicates that particle confinement remains nearly unchanged.

On the other side, we found in earlier studies, that HFS injection increases the bulk density while the separatrix region does not change significantly [19]. The reduced particle losses connected to HFS injection yield clear gain in plasma stored energy  $W_{MHD}$  in contrast to experiments with LFS injection [22], as demonstrated in Figure 6. The improvements are most pronounced at low heating powers. However, the confinement is still degraded with respect to extrapolations gained from scaling laws like the ITERH92-P scaling represented by the solid curves in Figure 6.

Notably, it should be mentioned that pellets can trigger neoclassical tearing modes [21] with detrimental effect on  $\tau_E$ . These modes are not observed in gas fuelled high-density discharges.

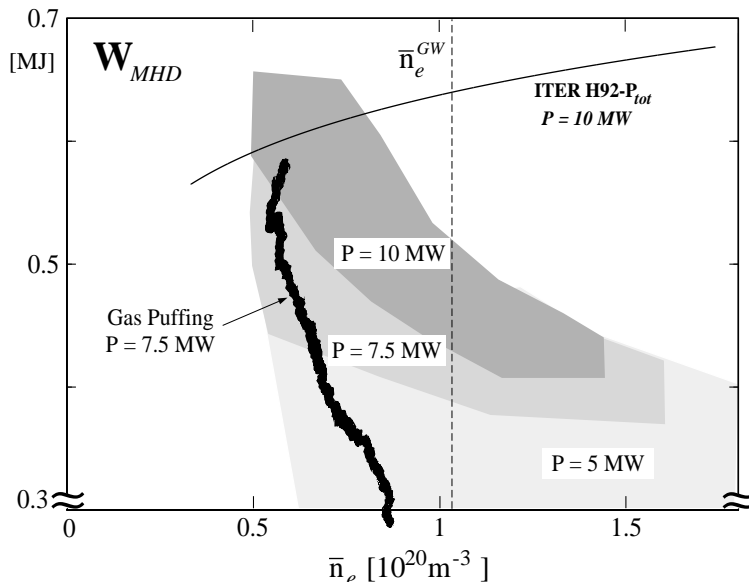


Figure 6: The shaded areas sketch the achieved operation space in plasma stored energy  $W_{MHD}$  and  $\bar{n}_e$  of stationary HFS pellet fuelled H-mode discharges at three different  $P_{heat}$ . A clear limitation towards high  $W_{MHD}$  and  $\bar{n}_e$  is seen which is not yet understood. For comparison a trajectory of a gas fuelled discharge is included. As reference the energy content of a 10 MW heated discharge is calculated (curve, ITERH92-P H-mode scaling).

A key element to understand the behaviour of pellet refuelled discharges described so far seems to be the evolution of density and temperature profiles. The measured evolution of electron density profiles with a ms temporal resolution gives no indication for a significant change of the gradient in the boundary region even for the time shortly after pellet injection. During the enhanced transport phase of fast density decay the loss from the plasma corresponds to a particle flux of about  $\Phi \approx 10^{22}/s$  crossing the edge region. As this flux is about one order of magnitude stronger than the fluxes usually encountered (e.g. a flux of  $10^{21}/s$  results at 10 MW NBI injection), we conclude that the diffusivity in the barrier region increases significantly during such phases as expected in a critical gradient situation. The excess density beyond that of purely gas fuelled discharges is caused by a radial broadening of the edge gradient zone into the plasma core. The central part of the profile remains almost flat.

The evolution of the electron temperature profile close to the plasma edge behaves like related gas-puffed discharges. A significant difference is observed, however, in the core region. In gas fuelled H-mode discharges with saturated edge pressure gradients (e.g. type-I ELMy H-mode) the temperature profiles show remarkable resilience [20]. When pellet injection sets in, the bulk temperatures drop below the according values. This contributes at least partially to the degradation of the plasma energy when  $\bar{n}_e$  is increased.

## 4. Summary

Systematic studies of H-mode density limit plasmas with gas fuelling and alternatively with additional pellet injection from the magnetic high-field-side HFS were performed in the new closed divertor configuration DV-II. The resulting database covering a wide range of the external controllable plasma parameters  $I_p, B_t$  and  $P_{heat}$  confirms that the H-mode threshold power exceeds dramatically the generally accepted prediction  $P_{heat}^{L \rightarrow H} \propto \bar{n}_e B_t$  when one approaches Greenwald densities. This makes it difficult to maintain the H-mode at high densities. In parallel, the large parameter variation revealed a moderate  $B_t$ -dependence of the H-mode density limit in contrast to the Greenwald scaling. This dependence can be reproduced by models which connect density saturation to divertor detachment [14]. The H-mode density limit is accompanied by detachment and a strong increase of the edge thermal transport inside the separatrix [7]. It is not yet clear what the actual cause of the H $\rightarrow$ L-backtransition is. Normally,  $\bar{n}_e \geq \bar{n}_e^{GW}$  is not obtained with gas fuelling.

On the other hand, pellet injection is able to surpass the Greenwald limit significantly in steady state. The new pellet injection scheme from the high-field-side, recently developed on ASDEX Upgrade, has significantly increased the pellet particle fuelling efficiency, especially at high heating powers.

It has been experimentally verified that the improved fuelling efficiency is caused by a diamagnetic drift of the pellet ablatant in major radius direction. While it drifts out from the confined plasma in the conventional low-field-side injection scheme, the ablatant moves favourably into the bulk during HFS injection. Nevertheless, additional particles losses connected with pellet injection like ELM induced losses and transient degradation of particle confinement still persist. With respect to the energy confinement a clear gain of the order of  $\leq 25\%$  is achieved. The reduction of this profit towards high heating powers, however, is not well understood. Further optimization can probably combine pellet injection with conserved high  $\tau_E$ .

## References

- [1] M. Greenwald et al., *Nuclear Fusion* **28**, (1988) 2199
- [2] P.T. Lang et al., *Phys. Rev. Lett.* **79** (1997) 1487
- [3] P.T. Lang, P. Cierpka, *Rev. Sci. Instr.* **69** (1998) 2806
- [4] F. Ryter et al., *Physica Scripta*, **51**, (1995) 643
- [5] H. Zohm, *Plasma Phys. Control. Fusion* **38**, 105 (1996)
- [6] W. Suttrop et al., PSI (1998), San Diego, USA
- [7] W. Suttrop et al., this conference, F1-CN-69/EXP2/6
- [8] B.N. Rogers et al., this conference, F1-CN-69/THP2/01
- [9] A. Zeiler et al., this conference, F1-CN-69/THP2/02
- [10] S.L. Milora, W.A. Houlberg, L.L. Lengyel, V. Mertens, *Nucl. Fusion* **35**, (1995) 657
- [11] M. Kaufmann, K. Lackner, L. Lengyel, and W. Schneider, *Nucl. Fusion* **27**, 171 (1986)
- [12] L.L. Lengyel, *Nucl. Fusion* **17**, (1977) 805
- [13] V. Mertens et al., *Nucl. Fusion* **37**, (1997) 1607
- [14] K. Borrass et al., *Contrib. Plasma Phys.*, **38**, (1998) 130
- [15] P.T. Lang et al., *Nucl. Fusion* **36** (1996) 657
- [16] J. Neuhauser et al., IPP Report 5/30 (November 1989)
- [17] J. Schweinzer et al., PSI (1998), San Diego, USA
- [18] P.B. Parks et al., *Nucl. Fusion* **17** (1977), 539
- [19] V. Mertens et al., *Controlled Fusion and Plasma Physics (Proc. 25rd Europ. Conf. Prague 1998)*, to be published
- [20] W. Suttrop et al., *Plasma Phys. Contr. Fusion* **39** (1997) 2051
- [21] M. Maraschek et al., submitted to *Plasma Phys. Control. Fusion*
- [22] V. Mertens et al., *Plasma Phys. Contr. Nucl. Fusion Research 1996 (Proc. 16. Int. Conf. Montreal, 1996)*, Vol. 1, IAEA, Vienna (1997) 413
- [23] S.L. Milora et al., *Nucl. Fusion* **35** (1995) 1531